Journal of Materials Chemistry C

Accepted Manuscript

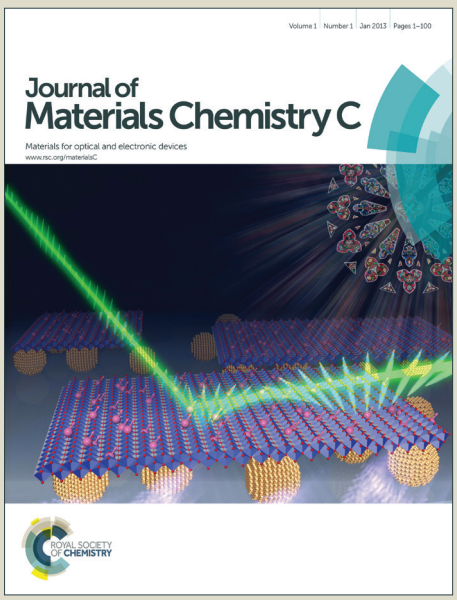

ROYAL SOCIETY OF CHEMISTRY

www.rsc.org/materialsC

Table of contents

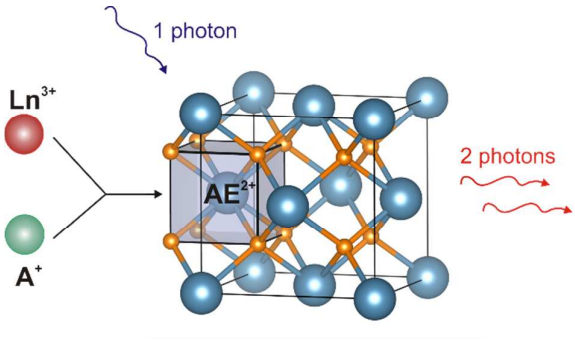

Careful charge compensation in doubly doped alkaline earth nanofluorides enables a luminescent material with 199 % quantum yield.

Journal Name

RSCPublishing

ARTICLE

Charge compensation in RE^{3+} (RE=Eu, Gd) and M^{+} (M=Li, Na, K) co-doped alkaline earth nanofluorides obtained by microwave reaction with reactive ionic liquids leading to improved optical properties

Cite this: DOI: 10.1039/x0xx00000x

Received 00th January 2012,
Accepted 00th January 2012

DOI: 10.1039/x0xx00000x

www.rsc.org/

C. Lorbeer,[a] F. Behrends,[b] J. Cybinska,[a,c] H. Eckert[b,d] and A.-V. Mudring[a,e*]

Alkaline earth fluorides are extraordinarily promising host matrices for phosphor materials with regard to rare earth doping. In particular, quantum cutting materials, which might considerably enhance the efficiency of mercury-free fluorescent lamps or SC solar cells, are often based on rare earth containing crystalline fluorides such as $NaGdF_4$, GdF_3 or LaF_3. Substituting most of the precious rare earth ions and simultaneously retaining the efficiency of the phosphor is a major goal. Alkaline earth fluoride nanoparticles doped with trivalent lanthanide ions (which are required for the quantum cutting phenomenon) were prepared via a microwave assisted method in ionic liquids. As doping trivalent ions into a host with divalent cations requires charge compensation, this effect was thoroughly studied by powder X-ray and electron diffraction, luminescence spectroscopy and ^{23}Na, ^{139}La and ^{19}F solid state NMR spectroscopy. Monovalent alkali ions were codoped with the trivalent lanthanide ions to relieve stress and achieve a better crystallinity and higher quantum cutting abilities of the prepared material. ^{19}F-magic angle spinning (MAS)-NMR-spectra, assisted by $^{19}F\{^{23}Na\}$ rotational echo double resonance (REDOR) studies, reveal distinct local fluoride environments, the populations of which are discussed in relation to spatial distribution and clustering models. In the co-doped samples, fluoride species having both Na^+ and La^{3+} ions within their coordination sphere can be identified and quantified. This interplay of mono- and trivalent ions in the CaF_2 lattice appears to be an efficient charge compensation mechanism that allows for improved performance characteristics of such co-doped phosphor materials.

Introduction

The alkaline earth fluorides MF_2 (M= Ca, Sr, Ba) are well known host materials for numerous applications in the field of scintillators and phosphor materials. Apart from benefits arising from the large band gap, the low phonon energy, and the relatively high pyrohydrolytic stability, alkaline earth fluorides are quite cheap owing to the large natural abundance of the alkaline earth salts.[1] Commonly, rare earth ions are doped into such matrices to create extrinsic luminescence. The introduction of trivalent lanthanide ions into the divalent alkaline earth fluoride lattice leads to the formation of solid solutions, in which the Ln^{3+} ion substitutes a M^{2+} ion and the initial cubic lattice persists.[2] However, the difference in charge between the trivalent lanthanide and the divalent alkaline earth ions requires compensation, potentially leading to defects such as interstitial fluoride ions and/or defect aggregation (often called "cluster formation"). Numerous studies of the charge compensating species and mechanism have been carried out by means of NMR, Raman, EPR, conductometry, dielectric losses, X-ray and neutron diffraction or luminescence spectroscopy, amongst others.[3-8] Nevertheless, contradictory results have been obtained and it has been realized that the resulting site symmetry of the lanthanide ion is strongly dependent on the nature of the alkali earth metal ion and the lanthanide ion, as well as on the dopant concentration. Additionally, the thermal history, oxygen impurities, and defects influence the charge compensation process.[2] The ideal site symmetry of the M^{2+} ion in the fluoride lattice is O_h. At low dopant ion concentrations, C_{4v} and C_{3v} site symmetries have been identified. For larger concentrations, the formation of rare earth enriched clusters was observed.[9-11] Efforts have been made to retain the O_h symmetry of the cation, and a good crystallinity, by co-doping with Li^+, Na^+ or K^+. Apart from an enhancement of rare earth ions in O_h symmetry,

additional sites of lower, C_{2v}, symmetry were produced.[12, 13] The effect on the (optical) properties can be significant as shown by Boulon et al. in Yb^{3+} and Na^+/K^+ codoped CaF_2 crystals.[14]

In contrast to the well-studied bulk materials (especially single crystals), reports on nanoscale alkaline earth fluorides doped with lanthanide ions or co-doped with lanthanide and alkali ions are scarce. The impact of the nanometer size regime on the particles' properties was demonstrated in a great variety of materials.[15- 17] Diverse measurable quantities as for instance the band gap, the conducting and luminescent properties can be affected.[18] Previously we reported on nanofluorides synthesized from ionic liquids (IL) with outstanding luminescent properties.[19- 21] Ionic liquids are excellent media for nanoparticle synthesis due to their unique stabilizing properties that rely on efficient electrostatic and steric stabilization. A fast and facile reaction procedure to impurity-free lanthanide fluorides in the microwave oven taking advantage of the extraordinary microwave susceptibility of ILs was developed by us.[22] The ionic liquid not only acts as a solvent and stabilizer, but also as a reactant providing the fluoride ion under decomposition at elevated temperatures. The universal application of this method was proven with the preparation of highly doped alkaline earth nanofluorides.[23] Therein, small particles of 5-20 nm size, depending on the reaction conditions, were obtained.

The aim of the work presented here is to study the effect of alkaline metal and rare earth metal co-doping on the structural, morphological and optical characteristics of the nanoparticles, in order to figure out the best property-performance correlation. To gain further insights into the structure and charge compensation mechanisms of the present materials, solid state NMR results are reported on nanocrystalline CaF_2 samples in which the Gd^{3+} and Eu^{3+} ions are replaced by diamagnetic La^{3+}, to avoid line broadening effects due to paramagnetic interactions and to introduce the ^{139}La isotope as an additional NMR probe. As NMR is an element-selective method sensitive to the details of local environments, it is well-suited for distinguishing different local environments present in crystalline solid solution systems. ^{19}F-magic angle spinning (MAS)-NMR was previously used for proving the random character of isovalent substitution in the CaF_2-SrF_2[24] and the CaF_2-BaF_2 systems.[25] In contrast, clear segregation and clustering phenomena were observed in the PbF_2-CdF_2 system.[26] Furthermore, a detailed ^{19}F MAS NMR study by Wang and Grey showed that aliovalent substitution in the CaF_2-YF_3 system creates multiple fluoride environments.[27] The quantitative concentrations of these environments have been discussed in relation to various defect cluster models originating from the necessary creation of interstitial fluoride ions owing to charge balancing constraints.[28-30] In the present study we present multinuclear NMR results on a series of CaF_2 nanoparticles co-doped with NaF and LaF_3. The results are compared to those of the corresponding singly doped (with NaF and LaF_3 only) materials and discussed in relation to the dopant distribution and the fluoride local environments in these samples.

Experimental

Synthetic procedures

Synthesis and sample handling were carried out under standard Schlenk and Argon-glove box techniques. 1-Methylimidazole (99 %, redistilled, Sigma Aldrich), chlorobutane (99 %, Acros), acetonitrile (99.5 %, J. T. Baker), sodium tetrafluoroborate (98 %, Aldrich), dichloromethane (99.9 %, Fisher Scientific), ethylene glycol (99 %, J. T. Baker) and ethanol (p.a., Sigma Aldrich) were used as received. Barium acetate (99 %), calcium acetate (99.9 %), lithium acetate (98 %), sodium acetate (98 %), potassium acetate (99 %), gadolinium acetate tetrahydrate (99.9 %) and europium acetate hydrate (99.99 %) were purchased from ABCR.

1-Methyl-3-butylimidazolium tetrafluoroborate, [C_4mim][BF_4]. The ionic liquid [C_4mim][BF_4] was synthesized in a two-step procedure with the quaternization of 1-methylimidazole and chlorobutane followed by an anion exchange reaction with $NaBF_4$. The reaction follows a common procedure and was described elsewhere.[19]

Nanoparticles. In a typical reaction the appropriate amounts of the acetate (hydrate) precursors were first dissolved in ethylene glycole and then mixed with an excess of [C_4mim][BF_4]. In a 10 ml glass vessel equipped with a Teflon septum, the reaction mixture was heated for 10 min at 120 °C in a single-mode microwave oven (2455 MHz, CEM Discover, Kamp-Lintfort, Germany). After cooling to room temperature by means of pressurized air, the obtained colloidal solution was centrifuged. The reaction product was washed several times with an ethanol/dichloromethane mixture. Finally, the colorless powder was dried at 70 °C.

Methods

Luminescence measurements. Fluorescence and lifetime measurements were carried out on a Fluorolog FL 3-22 spectrometer (Horiba Jobin Yvon, Unterhachingen, Germany). A continuous xenon lamp with 450 W for fluorescence and a pulsed xenon lamp for lifetime measurements (decay by delay) was applied. Double gratings for the excitation and emission spectrometer are used as monochromators. A photomultiplier detects the signal. For measurement, powdered samples were filled in silica tubes and carefully positioned in the incoming beam in the sample chamber. For measurements at liquid nitrogen temperature (77 K), a Dewar equipped with optical glass windows was used.

Powder X-ray diffraction. The powder X-ray diffraction measurements were carried out on a G670 diffractometer with an image plate detector (Huber, Rimsting, Germany) operating with MoKα radiation. The lattice parameters were refined with the program WinXPow (Stoe, Darmstadt, Germany).

Synchrotron radiation measurements. VUV spectroscopic measurements with synchrotron radiation were undertaken on

beamline I (SUPERLUMI station) at the Hamburger Synchrotronstrahlungslabor (HASYLAB), Deutsches Elektronensynchrotron (DESY), Germany. For more information see http://hasylab.desy.de/facilities/doris_iii/beamlines/e6259/index_eng.html or references 31 and 32.

Transmission electron microscopy. Transmission electron microscopy was carried out on a Tecnai G^2 20 X-Twin TEM (Fei, Hillsboro, USA) equipped with a Penta FET EDX detector (Oxford Instruments, UK). An acceleration voltage of 200 kV was applied. To prepare the samples, a suspension of the sample in ethanol was dropped on a copper grid coated with carbon and then dried in air.

Results and discussion

The effect of charge compensation in RE^{3+} (RE=Eu, Gd) and M^+ (M=Li, Na, K) co-doped BaF_2 nanoparticles was studied by examining two potential factors of influence: (a) the alkali metal cation (Na^+) concentration and (b) the type of alkali cation (Na^+ vs. Li^+ or K^+). Na^+ has an ionic radius of 1.32 Å and is thus of comparable size to Ca^{2+} or La^{3+}. Thus, it may be valid to assume a substitution of the alkaline earth metal ions by the alkali metal ion. Li^+ is with an ionic radius of 1.06 Å by far the smallest monovalent metal cation. On the other side, K^+ is with 1.65 Å the largest ion used for the preparation of the BaF_2: M^+, Gd^{3+}, Eu^{3+} nanomaterials herein. The overall lanthanide ion concentration (Gd^{3+} + Eu^{3+}) was kept equal to the alkali metal ion concentration to allow for an optimum charge compensation according to BaF_2: M^+ x %, Gd^{3+} (x-1) %, Eu^{3+} 1 %. The Eu^{3+} concentration is kept at 1 % to ensure both similar optical behavior and efficient energy transfer, and to avoid concentration quenching. A list of the samples is given in table 1.

Table 1. BaF_2: M^+ x %, Gd^{3+} (x-1) %, Eu^{3+} 1 % compositions studied.

Host	Gd^{3+} / %	Eu^{3+} / %	M^+ ion	M^+ / %
BaF_2	5	1	Na^+	6
BaF_2	15	1	Na^+	16
BaF_2	25	1	Na^+	26
BaF_2	5	1	Li^+	6
BaF_2	5	1	K^+	6

Host	La^{3+} / %	Na^+ / %
CaF_2	15	15
CaF_2	10	10
CaF_2	5	5
CaF_2	2	2
CaF_2	15	
CaF_2		15

Table 2. List of ionic radii for coordination number 8 for the cation and 4 for fluoride as observed in the fluorite structure. [34]

Ion	Ionic radius / Å
Ba^{2+}	1.56
Ca^{2+}	1.26
F^-	1.17
La^{3+}	1.30
Gd^{3+}	1.19
Eu^{3+}	1.21
Li^+	1.06
Na^+	1.32
K^+	1.65

Powder X-ray diffraction

The powder X-ray diffraction patterns of the BaF_2: Na^+, Gd^{3+}, Eu^{3+} samples with various dopant concentrations are displayed in figure 1. The cubic fluoride lattice is retained in all cases irrespective of the dopant concentration or the identity of the monovalent alkali metal ion. This is particularly interesting in the sample with dopant concentrations of 26 % Na^+, 25 % Gd^{3+} and 1% Eu^{3+}, where the overall amount of dopant ions is larger than that of the Ba^{2+} host cations. However, a significantly enhanced broadening of the reflections is observed when increasing the dopant concentrations from 6 % to 16 % and 26 % Na^+.

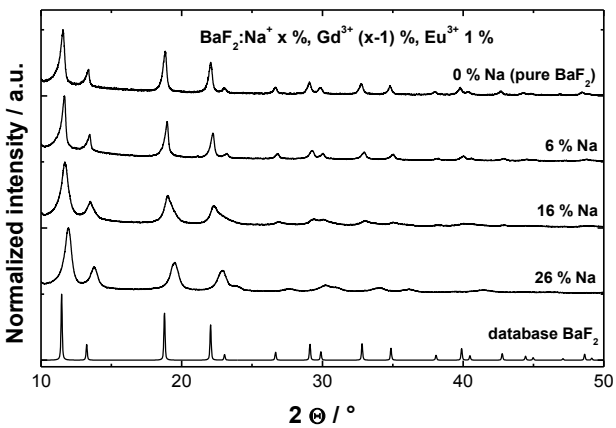

Figure 1. Powder X-ray diffraction patterns of samples with different concentrations of Gd^{3+}/Na^+ co-doped into BaF_2 and comparison with the simulated diffraction pattern for BaF_2.

Apart from the broadening, a systematic change in the lattice parameters is observed as anticipated from the ionic radii (see tables 2 and 3). The BaF_2: Gd^{3+} 5 %, Eu^{3+} 1% particles co-doped with 6% Li^+, Na^+ or K^+ (6.164 Å, 6.153 Å and 6.156 Å, respectively) have a lattice parameter in the expected range, similar to the lattice parameters of BaF_2:Gd^{3+} 5 %, Eu^{3+} 1% where no co-dopant alkali metal M^+ ions (6.159 Å) are present. Astonishingly, amongst all, the Li^+ co-doped material exhibits the largest lattice parameters, which seems to be in contradiction

to the small ionic radius of Li^+. As expected, an increase of the overall dopant concentration (Na^+ together with Gd^{3+} and Eu^{3+}) leads to reduced lattice parameters, which are close to the values obtained for the materials without Na^+ codoping.[23] Specifically, the lattice parameter *a* amounts to 6.147 Å for BaF_2: Gd^{3+} 15 %, Eu^{3+} 1% (compared to BaF_2: Na^+ 16 %, Gd^{3+} 15 %, Eu^{3+} 1% with *a*= 6.146 Å) and 6.135 Å for BaF_2: Gd^{3+} 25 %, Eu^{3+} 1% (to be compared with BaF_2: Na^+ 26 %, Gd^{3+} 25 %, Eu^{3+} 1% with *a*= 6.136 Å). Hence, the lattice parameter appears insensitive to co-doping by M^+ ions, which indicates that the structure is not significantly affected and the M^{2+} ions of the host lattice get cooperatively replaced by both, M^+ and M^{3+}. In case of interstitial M^+ ions (which are likely to be found in the tetrahedral voids provided by the anion lattice), the lattice parameter would be expected to change sensitively due to the difference in ionic radii. Thus, as Na^+ has a similar ionic radius as Gd^{3+} and Eu^{3+}, a coupled substitution mechanism, where Ln^{3+} and Na^+ ions are randomly substituting Ba^{2+} ions, appears to be likely. Such a mechanism should lead to a monotonic decrease of the lattice parameter with increasing dopant concentration as the dopant ions have a sizeably smaller radius than Ba^{2+}.

Table 3. Calculated lattice parameter *a* and cell volume (Vol_{cell}) of the synthesized BaF_2: M^+, Gd^{3+}, Eu^{3+} particles. The uncertainities amount to ± 0.001 or lower.

Sample	*a* / Å	Vol_{cell} / Å^3
BaF_2: Na^+ 6 %, Gd^{3+} 5 %, Eu^{3+} 1%	6.153	232.969
BaF_2: Na^+ 16 %, Gd^{3+} 15 %, Eu^{3+} 1%	6.146	232.030
BaF_2: Na^+ 26 %, Gd^{3+} 25 %, Eu^{3+} 1%	6.136	230.700
BaF_2: Li^+ 6 %, Gd^{3+} 5 %, Eu^{3+} 1%	6.164	234.161
BaF_2: K^+ 6 %, Gd^{3+} 5 %, Eu^{3+} 1%	6.156	233.270

The powder X-ray diffraction patterns of doped MF_2: $_x$ LaF_3, $_x$ NaF (M = Ca, Ba) samples are given in the Supporting Information. These samples containing the non-magnetic La^{3+} (in contrast to magnetic Eu^{3+} and Gd^{3+}) were prepared to allow for in-depth NMR studies. All materials crystallize in the cubic fluorite lattice, with no evidence for secondary phases. The corresponding lattice parameters are listed in table 4. Noticeably, the lattice parameters of the CaF_2 and BaF_2 nanocrystals solely doped with Na^+ (5.469 Å and 6.192 Å) are close to the lattice parameters of the database CaF_2 and BaF_2 materials (5.4631 Å and 6.2001 Å,[35] refinements of synthesized pure materials yielded 5.4634 Å and 6.2000 Å, respectively). No decrease of the lattice parameter was observed in Na-doped BaF_2 although the Na^+ ion is considerably smaller than the Ba^{2+} ion. This may suggest a failure of the incorporation of the Na^+ ions into the cubic BaF_2 lattice. Indeed only a very weak ^{23}Na solid state NMR signal was observed in these samples (*vide infra*).

Table 4. Calculated lattice parameters and cell volume of the AF_2: Na^+ 15% and AF_2: Na^+, La^{3+} particles (A= Ba, Ca) with various dopant concentrations. The uncertainities amount to ± 0.001 or lower.

Sample	a / Å	Vol_{cell} / Å
BaF_2	6.200	238.328
BaF_2: La^{3+} 15 %	6.131	230.459
BaF_2: Na^+ 15 %	6.192	237.460
BaF_2: Na^+ 2 %, La^{3+} 2 %	6.187	236.791
BaF_2: Na^+ 5 %, La^{3+} 5 %	6.186	236.716
BaF_2: Na^+ 10 %, La^{3+} 10 %	6.174	235.402
BaF_2: Na^+ 15 %, La^{3+} 15 %	6.148	232.382
CaF_2	5.463	163.040
CaF_2: La^+ 15 %	5.501	165.379
CaF_2: Na^+ 15 %	5.469	163.603
CaF_2: Na^+ 2 %, La^{3+} 2 %	5.467	163.398
CaF_2: Na^+ 5 %, La^{3+} 5 %	5.500	166.375
CaF_2: Na^+ 10 %, La^{3+} 10 %	5.492	165.650
CaF_2: Na^+ 15 %, La^{3+} 15 %	5.541	170.124

Transmission electron microscopy

To study the particle size and morphology of the synthesized material, transmission electron microscopy has been carried out. Representative micrographs are depicted in figure 2. The morphology of the synthesized alkali ion co-doped material (BaF_2: M, Gd, Eu) resembles the respective material without M^+ co-doping (BaF_2: Gd, Eu). The morphology of the alkali metal cation co-doped materials is similar to those without M^+. The BaF_2: M^+ 6 %, Gd^{3+} 5 %, Eu^{3+} 1 % particles (M= Li, Na, K) consist of two-dimensional plates tangled in each other as observed before for the BaF_2: Gd^{3+} 5 %, Eu^{3+} 1 % material.[23] The plate-like agglomerations consist of small particles with a mean size of 9.9 ± 1.8 nm and 9.2 ± 1.8 nm for the 5 % Na^+ and Li^+ co-doped material, respectively.

At higher dopant concentrations (BaF_2: Na^+ 26 %, Gd^{3+} 25 %, Eu^{3+} 1 %), particles with an average size of 9.1 ± 1.8 nm were obtained. The particle morphology is different in the highly concentrated sample. The particles cluster together yielding spherical, three-dimensionally dense agglomerations, which is again consistent with the morphology obtained for the solely 25 % Gd^{3+} and 1 % Eu^{3+} co-doped BaF_2 material. Nevertheless, a difference between the M^+ co-doped and M^+ free nanoparticles emerges from electron diffraction. Even at an overall dopant concentration of 52 % (BaF_2: Na^+ 26 %, Gd^{3+} 25 %, Eu^{3+} 1 %) a single crystalline diffraction pattern is observed in the materials doped with M^+ ions, whereas in the M^+-free particles, the material showed a polycrystalline character particularly with high dopant concentrations.

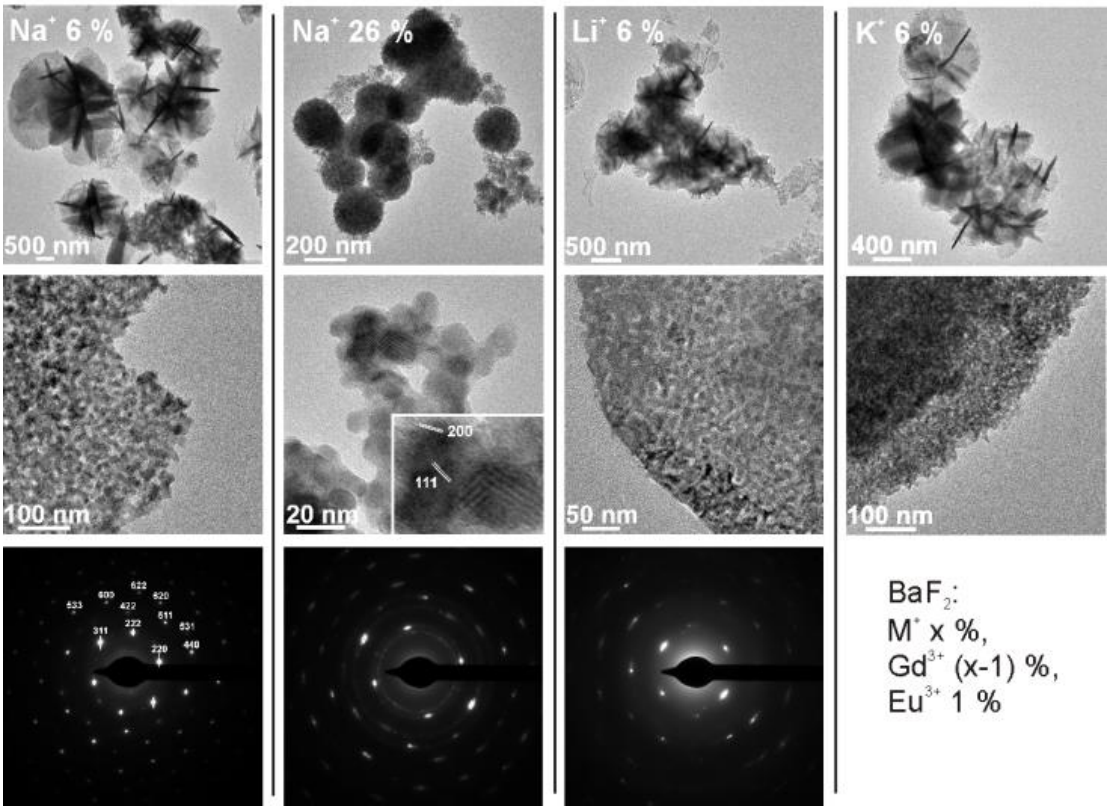

Figure 2. Representative TEM micrographs and electron diffraction of the BaF_2: Na x %, Gd (x-1) %, Eu 1 % particles.

Luminescence

The photo-physical properties of the synthesized materials were studied by luminescence spectroscopy. The room and low temperature emission spectra (λ_{ex}= 393 nm) of the BaF_2: Na^+, Gd^{3+}, Eu^{3+} particles with various dopant concentrations are depicted in figure 3. Orange-red Eu^{3+} emission originating from $^5D_{0,1} \rightarrow {}^7F_J$ can be observed, whereas no Gd^{3+} emission (which would occur around 310 nm) was monitored. Although all samples show similar emission features purely originating from Eu^{3+}, slight changes in the crystal field splitting with changing the dopant concentration are noticeable. Interestingly, the splitting is identical to those of the corresponding Na^+ free materials as far as it can be judged despite the broad lines. Amongst all, the 5 % Gd^{3+} and 1 % Eu^{3+} co-doped BaF_2 particles (with and without 6 % Na^+ co-doping) are significantly different from the particles with Gd^{3+} concentrations of 15 % and 25 % (each with and without corresponding Na^+ co-doping). The relative intensities of the emission originating from $^5D_1$ in comparison to $^5D_0$ change. With increasing dopant concentrations, the relative intensity of the $^5D_1 \rightarrow {}^7F_J$ emission increases, which is in agreement with the previously reported results on the Na^+-free particles. There, a dilution of the Eu^{3+} ions among the Gd^{3+} ions was given as an explanation which equals a lesser extent of concentration quenching. In addition, the relative intensity of the the $^5D_0 \rightarrow {}^7F_1$ with respect to the the $^5D_0 \rightarrow {}^7F_4$ transition differs. In fact, the $^5D_0 \rightarrow {}^7F_4$ transition shows an abnormally high intensity, which was previously reported to be due to slight distortions in highly polarizable environments.[36] However, the origin of this high intensity in the sample herein remains unsolved.

The emission spectra of the BaF_2: M^+ 6 %, Gd^{3+} 5 %, Eu^{3+} 1 % particles with different chemical identity of the monovalent M^+ ion are given in figure 4. In fact, all emission spectra are identical, with respect to the relative intensity of the $^5D_1$ emission and particularly the crystal field splitting. This indicates that the Eu^{3+} ion is residing in the same symmetry and coordination site.

The excitation spectra of all synthesized materials are given in the Supporting Information. They resemble the respective spectra of the M^+-free particles: The Gd^{3+} lines dominate the spectra, which suggests efficient $Gd^{3+} \rightarrow Eu^{3+}$ energy transfer.

Lifetimes

The luminescent lifetimes exciting directly into Eu^{3+} (λ_{ex}= 393 nm, λ_{em}= 590 nm) are given in table 5. Mono-exponential decay was observed for all samples presented herein. The lifetimes do not change significantly with increasing the dopant concentration or changing the M^+ ion (the error amounts to about 5 %). They resemble the lifetimes determined for the M^+-free particles (15.1-15.8 ms) with high dopant concentrations. However, the room temperature lifetime of the BaF_2: Gd^{3+} 5 %, Eu^{3+} 1% material amounts to 18.1 ms, which is significantly longer than the values obtained here for the M^+ co-doped material.

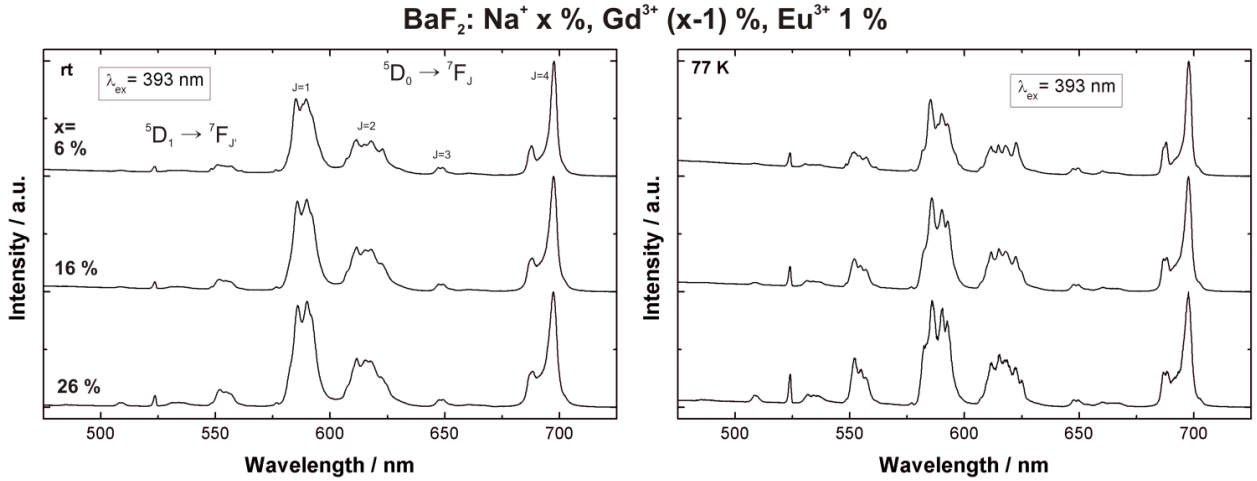

Figure 3. Emission spectra excited at λ_{ex}= 393 nm of BaF_2: Na^+, Gd^{3+}, Eu^{3+} particles with various dopant concentrations showing orange-red Eu^{3+} emission. The spectra were recorded at room temperature (left) and at 77 K (right).

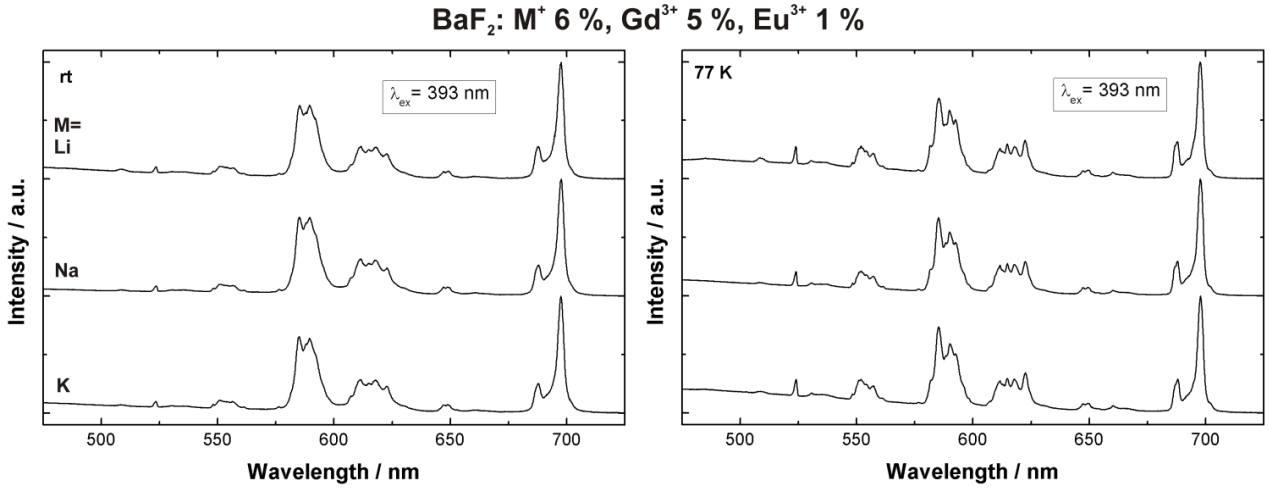

Figure 4. Emission spectra excited at λ_{ex}= 393 nm of BaF_2: M^+, Gd^{3+}, Eu^{3+} particles with M= Li, Na, K. The spectra were recorded at room temperature (left) and at 77 K (right).

Table 5. Luminescent lifetimes τ (λ_{ex}= 393 nm, λ_{em}= 590 nm) of the synthesized BaF_2: M^+, Gd^{3+}, Eu^{3+} particles recorded at room temperature (rt) and at liquid nitrogen temperature (77 K).

Sample	τ (rt) / ms	τ (77 K) / ms
BaF_2: Na^+ 6 %, Gd^{3+} 5 %, Eu^{3+} 1%	15.5	16.8
BaF_2: Na^+ 16 %, Gd^{3+} 15 %, Eu^{3+} 1%	15.9	17.4
BaF_2: Na^+ 26 %, Gd^{3+} 25 %, Eu^{3+} 1%	14.7	16.3
BaF_2: Li^+ 6 %, Gd^{3+} 5 %, Eu3+ 1%	16.1	17.1
BaF_2: K^+ 6 %, Gd^{3+} 5 %, Eu^{3+} 1%	14.9	15.2

VUV spectroscopy

To study the quantum cutting abilities, VUV excited emission spectra were recorded according to a common procedure.[37, 38] For this, the powdered samples are excited into Gd^{3+} levels at two different wavelengths. The obtained spectra excited at $^6G_J \leftarrow {}^8S$ (λ_{ex}= 202 nm), where quantum cutting is possible and at $^6I_J \leftarrow {}^8S$ (λ_{ex} = 274 nm) transition, where no quantum cutting can occur, are displayed in figure 5. It is important to notice that although exciting into Gd^{3+}, only Eu^{3+} emission is recorded due to efficient energy transfer. In all materials and irrespective of the dopant concentration or the chemical identity of the M^+ ion, quantum cutting occurs with a very high efficiency close to the theoretical limit of 200 %. The largest value of 199 % has been obtained for BaF_2: Na^+ 16 %, Gd^{3+} 15 %, Eu^{3+} 1%; while the Na^+-free counterpart exhibits a quantum cutting efficiency of only 172 %. This constitutes a significant increase of 27 %. Hence, the M^+ co-doped BaF_2: Gd^{3+}, Eu^{3+} particles represent substantially improved quantum cutting materials.

The results obtained from luminescence spectroscopy are consistent with the observations retrieved from X-ray diffraction. Two possible models can explain the obtained data. Firstly, the monovalent alkali ions have not been (or only to a small extent) incorporated into the BaF_2 lattice at all. This would explain the comparable lattice parameters, particle size and morphology of hypothetically M^+ doped and non-doped samples, and particularly with the identical emission spectra even when

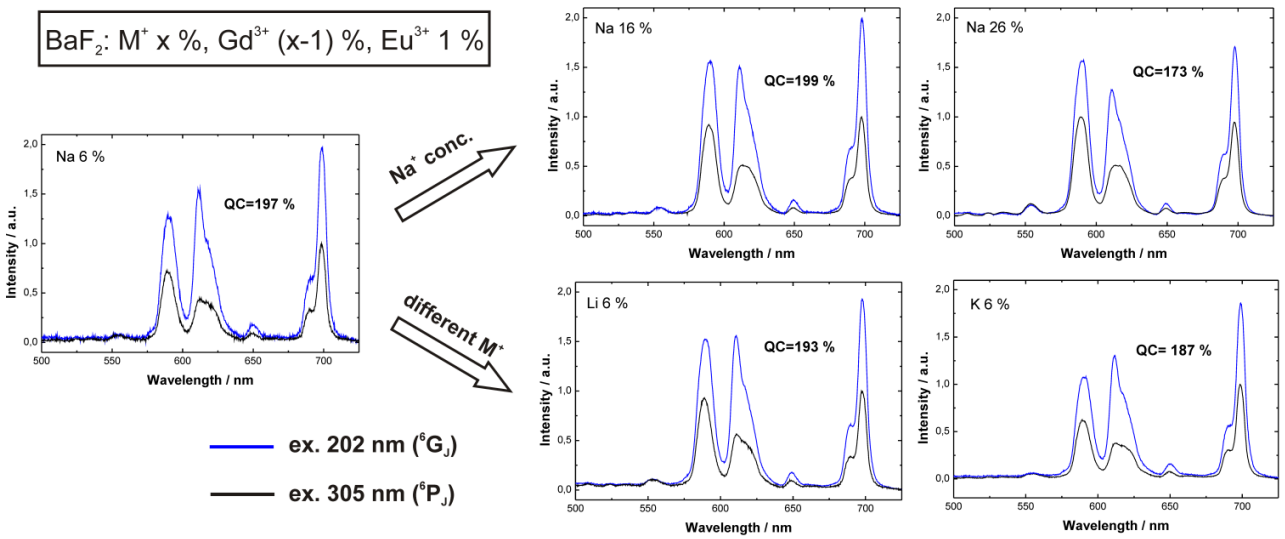

Figure 5. Room temperature emission spectra of BaF_2: M^+, Gd^{3+}, Eu^{3+} particles excited via $^6G_J \leftarrow {}^8S$ (λ_{ex} = 202 nm) and $^6I_J \leftarrow {}^8S$ (λ_{ex} = 274 nm) to check for quantum cutting abilities. The spectra are normalized on the $^5D_1$ emission and the calculated quantum cutting efficiencies are given in the right top corner.

exchanging the differently sized M^+ ions in comparison to the M^+-free particles. However, the close to 100% yield of the particle synthesis contradicts this hypothesis, particularly as no evidences for LiF, NaF or KF phases have been observed in the XRD patterns.

Secondly, a coupled substitution mechanism as described in the introduction, wherein the M^+ ion substitutes a Ba^{2+} ion in nearest neighbor cubic coordination to the Eu^{3+} ion, may explain the data in accordance with the similar sizes of the Na^+, Gd^{3+} and Eu^{3+} ions. Particularly at a high doping level of up to 25% Gd^{3+}, such a coupled substitution mechanism might lead to a higher crystallinity as a large number of interstitial fluoride ions would severely disturb the lattice order. The single crystalline electron diffraction patterns support this assumption. In addition, the lifetime of the BaF_2: Na^+ 6 %, Gd^{3+} 5 %, Eu^{3+} 1 % particles is shortened in comparison to the Na^+-free counterpart, which further backs this finding. To confirm that a cooperative charge compensation mechanism is taking place by substituting jointly divalent alkaline earth cations by monovalent alkali metal and trivalent lanthanide ions in the fluoride lattice, solid state NMR spectroscopic studies were carried out on CaF_2: La x %, Na x% materials in order to prevent interactions of the paramagnetic Gd.

Solid-State NMR

Figure 6 shows the ^{23}Na-MAS-NMR-spectra of four different CaF_2 based samples. These spectra prove that sodium ions are indeed incorporated into the lattice and the obtained intensity per scan confirms that the amount of sodium increases with increasing sodium content provided in the synthesis. In contrast, only very weak ^{23}Na-NMR signals of the doped BaF_2 samples could be obtained, indicating that Na^+ incorporation was less successful, which is in accordance with the X-ray powder diffraction data.

The spectrum of the singly doped CaF_2: 15% Na sample is the only one that shows a minor resonance at 7.2 ppm that can be attributed to residual $NaBF_4$ from the synthesis. This sample also shows a ^{1}H-MAS-NMR-spectrum (see Supporting Information

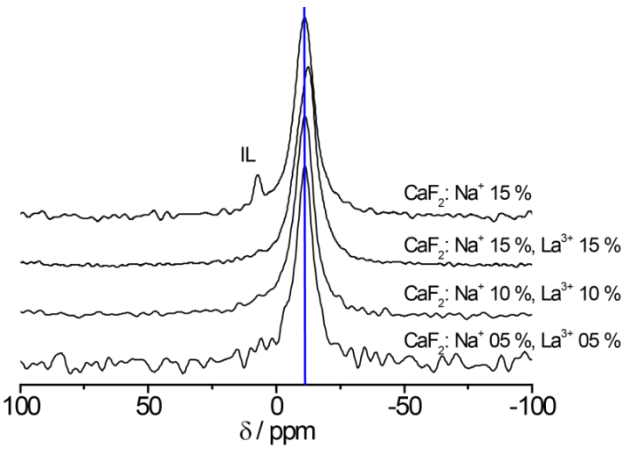

Figure 6. ^{23}Na-MAS-NMR-spectra of four different sodium containing CaF_2-samples.

Section) that identifies the ionic liquid starting material as an impurity. The spectra of all the samples are dominated by a peak centered around -11 ppm. This gives strong evidence that only one type of sodium site is present in the lattice and that its chemical environment is the same in all the samples under study. The center of gravity in the co-doped samples is shifted to slightly lower frequencies as the degree of doping is increased. Also, there is a slight chemical shift difference between the CaF_2:

Na^+ 15 % and the CaF_2: Na^+ 15 %, La^{3+} 15 % samples suggesting that the sodium ions experience the presence of the RE-ions in the lattice as well. The absence of any notable influence of second order quadrupolar perturbation effects on the ^{23}Na-MAS-NMR line shape indicates that the sodium atoms must be located in a highly symmetric environment that is most likely the cubic site of the alkaline earth ions they replace. This is in agreement with the information obtained from X-ray powder diffraction, indicating no significant change in lattice parameter.
Finally, the ^{23}Na spin echo decay rates of CaF_2: Na 15 % and CaF_2: Na 15 %, La 15 % samples are found to be identical within experimental error, which is consistent with similar spatial distributions of the Na^+ ions in both materials (see Supporting Information Section).

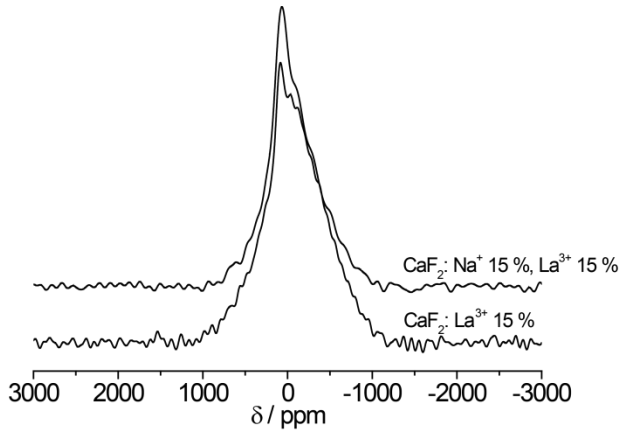

Figure 7. Static ^{139}La-NMR-spectra of the singly and doubly doped CaF_2 nanocrystals containing 15 % La.

Figure 7 depicts the static ^{139}La-NMR-spectra for the CaF_2 nanocrystals that were either singly doped with 15 % La^{3+}or co-doped with 15 % La^{3+} and 15 % Na^+. The spectra suggest that the La^{3+} environments are essentially the same in the doped and the co-doped samples. The relatively symmetric line shapes suggest weak quadrupolar coupling as expected for a slightly distorted pseudo-cubic coordination environment, which is expected if La^{3+} occupies the cation sites in the fluorite lattice.
More detailed information about the local environments are accessible through ^{19}F-MAS-NMR-experiments. Results were obtained both on samples doped exclusively with Na^+ and La^{3+} as well as on co-doped samples. Figure 8 shows the ^{19}F-MAS-NMR-spectrum of the CaF_2 sample doped with 15 % Na^+. The spectrum can be fitted using two signal components. One main resonance is centered at -107 ppm, the frequency found for the corresponding undoped material, and a second signal component near -114 ppm (labeled F' in Figure 8), which may be attributed to fluoride ions that have at least one sodium atom in the first coordination sphere. In addition, a minor resonance in the range of -140 to -155 ppm is visible, which can be attributed to residual fluoride from the ionic liquid precursor. No signal of a separate NaF phase can be found (which would be expected at -224 ppm), and its formation can thus be ruled out.

The fractional signal area of the unperturbed resonance representing the regular fluoride sites is 0.7. For a statistical distribution of Na over the CaF_2 lattice, a fractional area of $(0.85)^4 = 0.52$ would be expected. The deviation from this result is consistent with the idea of some clustering of the sodium ions (see further discussion below).

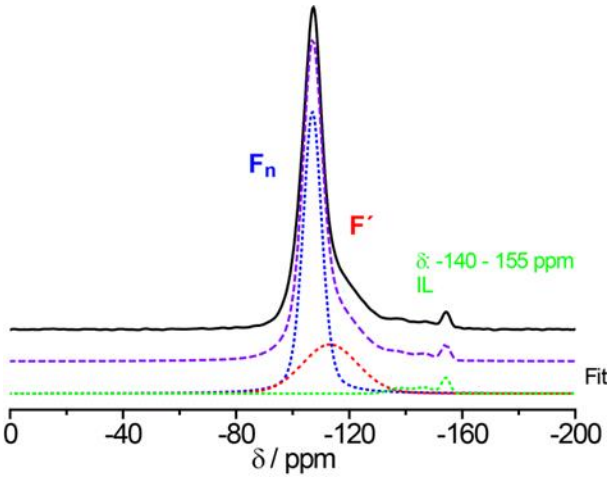

Figure 8. ^{19}F-MAS-NMR-spectra and corresponding lineshape deconvolution for singly doped CaF_2: Na^+ 15 %.

The ^{19}F-MAS-NMR-spectra of the CaF_2 nanocrystals doped with 15% La^{3+} are depicted in Figure 9. Multiple resonances are observed.

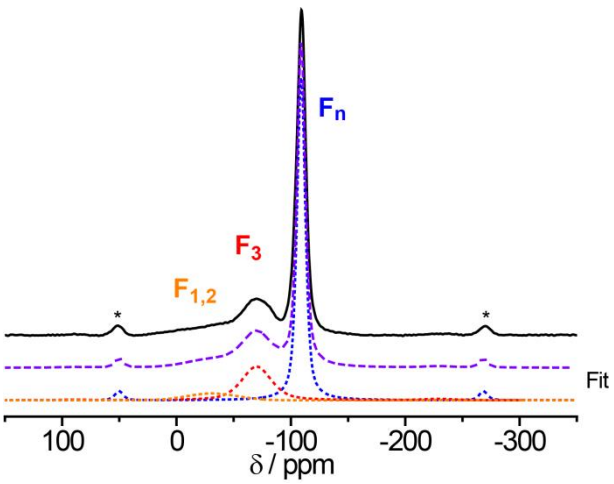

Figure 9. ^{19}F-MAS-NMR-spectra and corresponding lineshape deconvolution for singly doped CaF_2: La^{3+} 15 %.

Table 6 summarizes the results from the peak deconvolutions. Again the dominant signal at -109 ppm can be assigned to those ^{19}F nuclei belonging to the unperturbed host lattice itself, and are thus exclusively surrounded tetrahedrally by Ca^{2+} ions. For the assignment of the other resonances we follow the study of Wang and Grey, who published analogous ^{19}F-MAS-NMR data for Y-doped polycrystalline CaF_2 samples.[27] In that study, aliovalent doping with Y^{3+} was shown to give rise to four ^{19}F resonances,

which were assigned in relation to various defect cluster models.[28-30] Two distinct interstitial fluoride sites, labeled F_1 and F_2, both of which have two Y^{3+} nearest neighbors, a perturbed regular site F_3, which is slightly displaced from its regular lattice site position, owing to the interaction with one Y^{3+} nearest neighbor, and the normal site F_n that is unperturbed by the proximity of any dopant ion. The spectrum of our CaF_2: 15 % LaF_3 sample shows a similar general appearance. Besides the "regular" signal near -109 ppm, two broad signals at -70 and -31 ppm are found. The first one can be considered analogous to that of the F_3 site and is thus tentatively attributed to fluoride ions next to one La^{3+} species, while the resonance near -31 ppm might be assignable to interstitial fluoride ions, resembling the F_1 and/or F_2 sites reported in reference 26 and having proximity to two lanthanum species. Based on these assignments, we observe that the signal displacements relative to F_n are generally larger here than those in Y-doped CaF_2. This effect might be attributable to the fact that the larger La^{3+} ion causes stronger structural perturbations than the Y^{3+} ion.

Finally, even though the spectrum shows intensity in the frequency range where the two ^{19}F-resonances of LaF_3 resonate (see SI), the characteristic ^{19}F-NMR line shape of this phase cannot be identified, thus ruling out this kind of secondary phase formation.

The area fraction of the unperturbed signal F_n signal (69 %) is significantly higher than that expected for a statistical distribution (52.2 %), consistent with clustering. The area ratios can be compared with the various types of clustering scenarios examined for Y-doped CaF_2[27] and it is found that the experimentally observed peak intensities are in good agreement with the <110> F_1 pair model.

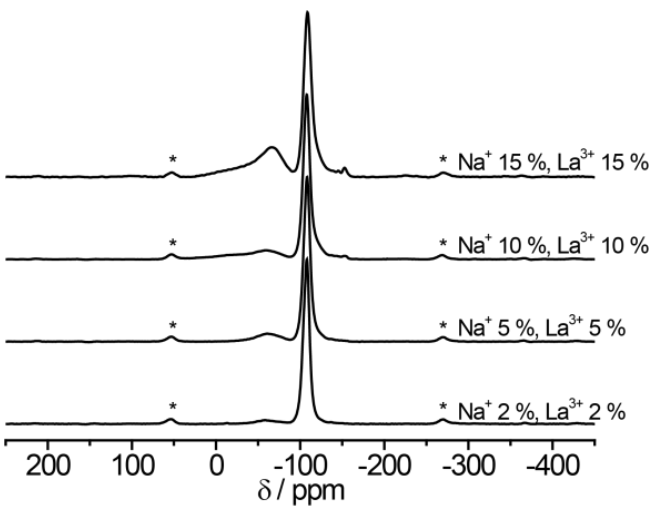

Figure 10. ^{19}F-MAS-NMR-spectra recorded in dependence of the degree of co-doping for the CaF_2 nanocrystals.

With the knowledge obtained so far, the spectra of the co-doped samples can be now discussed. Figure 10 shows the ^{19}F-MAS-NMR-spectra as a function of co-doping level, and Figure 11 shows a deconvolution of the ^{19}F-MAS-NMR-spectrum of the CaF_2: Na^+ 15 %, La^{3+} 15 % sample. The deconvolution deconvolution parameters of all samples are summarized in Table 6.

Table 6. ^{19}F-MAS-NMR lineshape deconvolution parameters for the CaF_2-nanocrystals under study.

Sample	Signal	δ ± 0.2 / ppm	FWHM ± 0.2 / ppm	Area ± 0.5 / %
CaF_2: Na^+ 15 %	F_n	-107.1	7.9	69.8
	F´	-113.9	23.2	30.2
	F_3	-	-	-
	$F_{1,2}$	-	-	-
CaF_2: La^{3+} 15 %	F_n	-109.0	8.6	68.5
	F´	-	-	-
	F_3	-70.0	30.8	24.9
	$F_{1,2}$	-31.1	51.6	6.6
CaF_2: Na^+ 15 % La^{3+} 15 %	F_n	-108.4	10.1	45.8
	F´	-117.0	20.6	14.5
	F_3	-66.5	30.0	25.5
	$F_{1,2}$	-31.6	57.3	14.2
CaF_2: Na^+ 10 % La^{3+} 10 %	F_n	-107.7	8.9	71.3
	F´	-116.7	19.0	9.7
	F_3	-61.5	31.0	8.9
	$F_{1,2}$	-27.0	60.45	10.1
CaF_2: Na^+ 5 % La^{3+} 5 %	F_n	-108.1	8.9	84.6
	F´	-116.2	18.3	4.7
	F_3	-62.1	27.7	9.3
	$F_{1,2}$	-37.6	26.73	1.4
CaF_2: Na^+ 2 % La^{3+} 2 %	F_n	-107.6	8.3	92.8
	F´	-114.4	20.3	2.6
	F_3	-58.8	26.7	4.6
	$F_{1,2}$	-	-	-

The spectra of the co-doped compounds appear to be superpositions of those of the singly doped samples, suggesting that the structural perturbations observed in the CaF_2 lattice are basically the same for the co-doped and for the singly doped samples. Again, important structural information is available from the peak area ratios. If both species were distributed statistically in the host material, the center signal should comprise only $(0.7)^4$*100 = 24 % of the overall intensity. Clearly, this is not the case, indicating some extent of clustering. The high frequency signals associated with fluorine in the vicinity of La now comprise 39.7 % of the overall signal intensity while 14.5 % of the F have just sodium as a dopant ion in their first coordination sphere. Assuming the amounts of Na^+ and La^{3+} to be equal, the question arises, whether the high-frequency resonances represent, at least in part, fluoride ions that are, besides to La^{3+}, also coordinated to Na^+ ions. This question can be examined on the basis of the heteronuclear dipole-dipole

interaction between ^{19}F and ^{23}Na as probed using $^{19}F\{^{23}Na\}$-REDOR. A handicap encountered with this particular experiment is the rather strong homonuclear dipolar coupling between the ^{19}F-spins, which causes the rotor synchronized spin echo intensity recorded in REDOR to decay rather quickly, diminishing the signal to noise ratio already at rather short dipolar evolution times. Nevertheless, a clear result could be obtained for a dipolar evolution time of 0.9 ms.

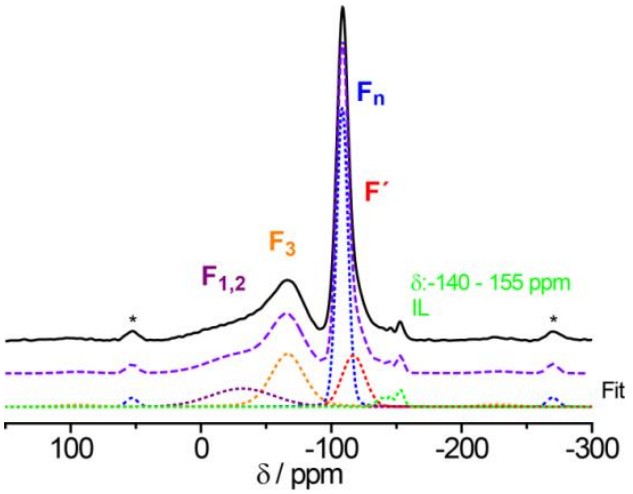

Figure 11. ^{19}F-MAS-NMR-spectrum and deconvolution of the experimental line shape for CaF_2: Na^+ 15 %, La^{3+} 15 %.

Figure 12 shows that the main resonance near -108 ppm remains unperturbed, while the intensity of the -117 ppm resonance is strongly decreased through the ^{23}Na recoupling effect as expected ($\Delta S/S_0$ = 0.38). The most interesting information, however, is the noticeable dephasing of the high frequency resonance under these conditions ($\Delta S/S_0$ = 0.16), indeed suggesting that at least part of these fluorine atoms are coordinated by both the La^{3+} and the Na^+ dopant species. We conclude that in CaF_2: Na^+ 15 %, La^{3+} 15 % there are a substantial number of fluoride species having both Na^+ and La^{3+} cations within their first coordination spheres. Proximal Na^+ and La^{3+} ions in the fluorite lattice do neither require interstitial fluoride ions nor fluoride vacancies, thereby opening up an additional charge balancing mechanism in such co-doped samples. On the other hand, the sizeable contribution of the F' resonance at -117 ppm suggests that there are significant fractions of fluoride species coordinating with La^{3+} or Na^+ alone, indicating that Na^+/La^{3+} co-doping produces no strong spatial correlations between both species.

Furthermore, a comparison of Figure 9 with Figure 11 and inspection of Table 6 reveals the expected behavior that the ratio of the area of the -32 ppm peak to the area of the -65 ppm peak is substantially higher in the co-doped sample than in the singly doped sample. According to our assignment, the -32 ppm peak represents fluoride species having two (or more) rare earth ions within their first coordination sphere. The increased concentration of these fluoride species indicates that in the co-doped samples, the number of rare earth ions interacting with a second RE-ion is significantly higher in the CaF_2: Na^+ 15 %, La^{3+} 15 % sample than in the CaF_2: La^{3+} 15 % sample alone. The more pronounced proximity of the rare earth ions in the co-doped sample is in excellent agreement with the experimental observation that quantum cutting ability is increased through co-doping. Thus, the NMR results support the idea that co-doping with alkaline ions opens a new mechanism route for charge compensation for the RE-ions and enhancing the quantum cutting performance.

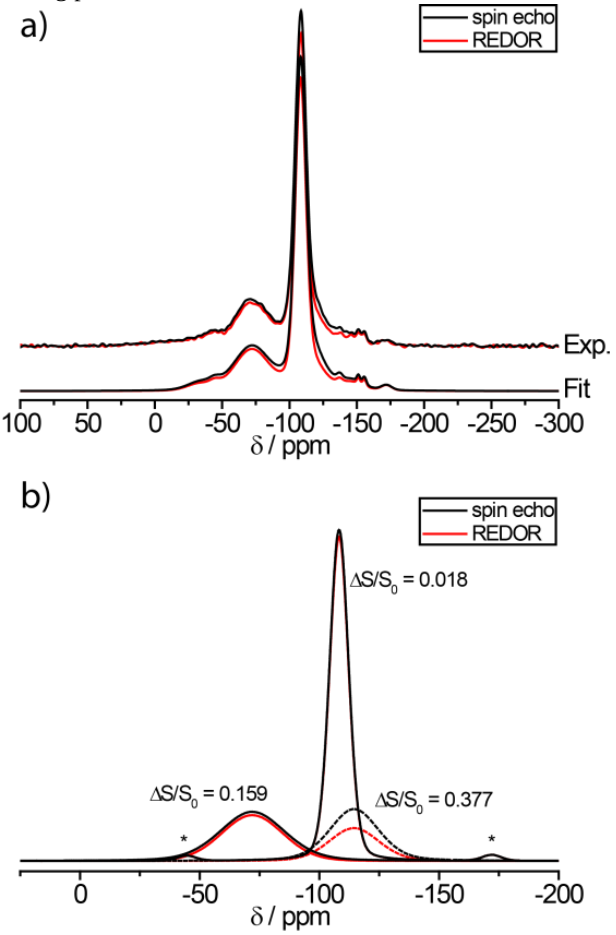

Figure 12. Comparison of the ^{19}F-MAS-NMR-spectra obtained on nanocrystalline CaF_2: La 15 %, Na 15 % by $^{19}F\{^{23}Na\}$-REDOR for a dipolar recoupling time of 0.9 ms (a), and the respective deconvolutions of the lineshape into individual contributions with and without recoupling of the hetero nuclear interaction (signal intensities S and S_0) (b).

Conclusion

Using a new ionic liquid-based preparation route, alkaline earth fluoride nanoparticles doped simultaneously with trivalent lanthanide ions and monovalent alkali ions were prepared. Whilst the lanthanide ions, Gd^{3+} and Eu^{3+}, served as the optical active centers allowing for quantum cutting, co-doping with mono-valent ions allowed to increase the homogeneity of the material in comparison to materials solely doped with trivalent ions. The charge compensation mechanism was elucidated by a

multi-analytical approach using powder X-ray diffraction, electron microscopy, electron diffraction, luminescence spectroscopy and various solid state NMR techniques. Specifically, ^{19}F solid state NMR spectra, assisted by $^{19}F\{^{23}Na\}$ REDOR experiments allow an identification and quantification of those fluoride ions that are coordinated simultaneously to both alkali and lanthanide ions. NMR data show that no evidence for strong Na···La spacial correlation, but, an increase for La···La which is important for the cooperative optical effect necessary for quantum cutting. In consequence, the induced charge compensation mechanism by simultaneous co-doping with rare earth and alkali metal ions favors efficient quantum-cutting. Amazingly, the rare earth content (cation content) could be reduced by 94 % compared to the typical GdF_3:Eu VUV quantum cutting material while simultaneously retaining the quantum cutting efficiency close to the theoretical limit (199 %).

Acknowledgements

This work was supported in part by the Critical Materials Institute, an Energy Innovation Hub funded by the U.S. Department of Energy, Office of Energy Efficiency and Renewable Energy, Advanced Manufacturing Office and the European Research Council with an ERC starting grant ("EMIL", contract no. 200475). A.-V. M. thanks the Fonds der Chemischen Industrie for a Dozentenstipendium, C. L. and F. B. thank the Fonds der Chemischen Industrie for doctoral scholarships. DESY (proposal no. II-20090181) is acknowledged for access to synchrotron facilities. H.E. is grateful for funding by FAPESP, grant number 2013/07793-6 (CERTEV – Center for Research, Technology and Education in Vitreous Materials).

Abbreviations

AE, alkaline earth; RE, rare earth; IL, ionic liquid, NMR, nuclear magnetic resonance, MAS, magic angle spinning, REDOR, rotational echo double resonance

Notes and references

[a] Ruhr-Universität Bochum, Inorganic Chemistry III-Materials Engineering and Characterization, Universitätsstraße 150, D-44780 Bochum, Germany.

[b] Westfälische Wilhelms-Universität Münster, Institut für Physikalische Chemie, Corrensstr. 28/30, D-48149 Münster, Germany

[c] University of Wrocław, Faculty of Chemistry, Joliot-Curie 14, 50383 Wrocław, Poland.

[d] University of Sao Paulo, Institute of Physics, Av. Trabalhador Saocarlense, Sao Carlos, Brazil.

[e] Ames Laboratory, Critical Materials Institute, and Iowa State University, Ames, IA, USA. E-mail: mudring@iastate.edu.

Electronic Supplementary Information (ESI) available: Excitation spectra, NMR spectra and additional powder X-ray diffraction patterns. See DOI: 10.1039/b000000x/

1 S. V. Kuznetsov, V. V. Osiko, E. A. Tkatchenko, P. P. Fedorov, Russ. *Chem. Rev.*, 2006, **75**, 1065.

2 B. P. Sobolev, A. M. Golubev, P. Herrero, *Cryst. Reports*, 2003, **48**, 141.

3 U. Ranon, A. Yaniv, *Phys. Lett.*, 1964, **9**, 17.

4 M. Kolesik, B. Sobolev, *Solid State Ionics*, 1991, **47**, 325.

5 Y. Kirsh, N. J. Kristianpoller, *J. Phys. Paris*, 1976, **7**, 216.

6 C. R. A. Catlow*J. Phys. C*, 1976, **9**, 1845.

7 C. R. A. Catlow, *J. Phys. C*, 1976, **9**, 1859.

8 J.-P. R. Wells, T. Dean, R. J. Reeves, *J. Lumin.*, 2002, **96**, 239.

9 J. P. Jouart, C. Bissieux, G. Mary, *J. Lumin.*, 1987, **37**, 159.

10 A. Gektin, N. Shiran, V. Nesterkina, Y. Boyarintseva, V. Baumer, G. Stryganyuk, K. Shimamura, E. & Villora, *J. Lumin.*, 2009, **129**, 1538.

11 B. P. Sobolev, A. M. Golubev, L. P. Otroshchenk, V. N. Molchanov, R. M. Zakalyukin, E. A: Ryzhova, P. Herrero, *Cryst. Reports*, 2003, **48**, 944.

12 L. van Pieterson, R. P. A. Dullens, P. S. Peijzel, A. Meijerink, G. D. Jones, *J. Chem. Phys.*, 2001, **115**, 9393.

13 G. D. Jones, R. J. Reeves, *J. Lumin.*, 2000, **87**, 1108.

14 S. Hraiech, A. Jouini, K. J. Kim, Y. Guyot, A. Yoshikawa, G. Boulon, *Radiat. Meas.*, 2010, **45**, 323.

15 A. Henglein, *Chem. Rev.*, 1989, **89**, 1861.

16 R. S. Meltzer, S. P. Feofilov, B. Tissue, H. B. Yuan, *Phys. Rev. B*, 1999, **60**, R14 012.

17 J. Suyver, R. Meester, J. J. Kelly, A. Meijerink, *J. Lumin.*, 2003, **102**, 182.

18 G. Liu, X. Chen, J.-C. Bünzli, V. K. Pecharsky, V. K. (ed.) *Spectroscopic Properties of Lanthanides in Nanomaterials*, in Handbook of the Physics and Chemistry of Rare Earths Vol. 37, ch. 233, Elsevier, Amsterdam, the Netherlands, **2007**.

19 C: Lorbeer, J. Cybinska, A.-V. Mudring, *Cryst. Growth Des.*,, 2011, **11**, 1040.

20 P. Ghosh, S.-F. Tang, A.-V. Mudring, *J. Mater. Chem.*, 2011, **21**, 8640.

21 Q: Ju, A.-V. Mudring, *RSC Advances*, 2013, **3**, 8172-8175.

22 C. Lorbeer, J. Cybinska, A.-V. Mudring, *Chem. Commun.*, 2010, **46**, 571.

23 C. Lorbeer, J. Cybinska, E. Zych, A.-V. Mudring, *Opt. Mater.*, 2011, **34**, 336.

24 R. E. Youngman, C. M. Smith, *Phys. Rev. B*, 2008**, 78**, 014112.

25 A. Düvel, B. Ruprecht, P. Heitjans, M. Wilkening, *J. Phys. Chem. C*, 2011, **115**, 23784.

26 A. Picinin, R. R. Deshpande, A. S. S. de Camargo, J. P. Donoso, J. P. Rino, H. Eckert, M. A. P. Silva, *J. Chem. Phys*., 2008, **128**, 224705.

27 F. Wang, C. P. Grey, *Chem. Mater*., 1998, **10**, 3081

28 A. K. Cheetham, B. E. F. Fender, D. Steele, R. I. Taylor, B. T. M. Willis, *Solid State Commun*., 1970, **8**, 171.

29 A. K. Cheetham, B. E. F. Fender, M. J. Cooper, *J. Phys. C: Solid State Phys*., 1971, **4**, 3107.

30 J. P. Laval, A. Mikou, B. Frit, *Solid State Ionics*, 1988, **28-30**, 1300.

31 G. Zimmerer, *J. Lumin.*, 2006, **119**, 1.

32 G. Zimmerer, *Radiat. Meas.*, 2007, **42**, 859.

33 D. Massiot, F. Fayon, M. Capron, I. King, S. LeCalvé, S.; Alonso, B.; Durand, J.-O.; Bujoli, B.; Gan, Z.; Hoatson, G. *Magn. Reson. Chem.*, 2002, **40**, 70-76.

34 R. D. Shannon, *Acta Cryst. A*, 1976, **32**, 751.

35 Lattice parameters retrieved from PDF-2 database. PDF 35-816 for CaF_2 and PDF 4-452 for BaF_2.

36 R. A. Sá Ferreira, S. S. Nobre, C. M. Granadeiro, H. I. S. Nogueira, L. D. Carlos, O. L. Malta, *J. Lumin.*, 2006, **121**, 561.
37 R. T. Wegh, H. Donker, U. D. Oskam, A. Meijerink, *Science*, 1999, **283**, 663.
38 C. Lorbeer, J. Cybinska, A.-V. Mudring, *J. Mater. Chem. C*, 2014, **2**, 1862.

